applied sciences

MDPI

Article

Effects of New Tunnelling on a Buried Pipeline with Joints and Its Detachment

Ye Dong [1], Xiang Liu [2,*], Rui Zhang [2] and Chengyong Yang [1]

[1] Department of Civil Engineering, Beijing Jiaotong University, Beijing 100044, China; vivilover@live.com (Y.D.); chyyang@bjtu.edu.cn (C.Y.)
[2] Liaoning Key Laboratory of Marine Environmental Bridge and Tunnel Engineering, Dalian Maritime University, Dalian 116026, China; ray@dlmu.edu.cn
* Correspondence: xliu@dlmu.edu.cn; Tel.: +86-(0)411-8472-4258

Abstract: The interactions between the buried pipeline and tunnelling-induced ground movement are studied in this paper, in which the jointed pipeline, Pasternak foundation, and the detachment are considered. A mathematical model using the pulse function is provided to simplify the jointed pipeline to a continuous pipeline with additional local rotations. The determination of detachment is used by the usual iteration method. The finite difference method is utilized to obtain the numerical results. The results calculated by our proposed method agree with the experimental data of centrifuge tests and are close to those obtained by the other methods. The deflection and bending moment of the jointed pipeline can be predicted reasonably, as well as its detachment location. Parametric analyses about the main influencing factors are carried out. The stiffness reduction factor is significant to the discontinuous behavior of the jointed pipeline. During the parametric analyses, the detachment beneath the jointed pipeline sometimes happens and sometimes does not. The responses of the jointed pipeline and its detachment require priority attention.

Keywords: jointed pipeline; Pasternak foundation; detachment; finite difference method

Citation: Dong, Y.; Liu, X.; Zhang, R.; Yang, C. Effects of New Tunnelling on a Buried Pipeline with Joints and Its Detachment. *Appl. Sci.* **2022**, *12*, 3342. https://doi.org/10.3390/app12073342

Academic Editor: Ricardo Castedo

Received: 1 March 2022
Accepted: 22 March 2022
Published: 25 March 2022

1. Introduction

With the extraordinary increase in population and subsequent transport networks, the construction of infrastructure involving underground excavations is undergoing an uncommon period of prosperity. Such excavations inevitably cause ground movements, leading to the longitudinal responses of buried pipelines. Research shows that the primary causes of fractures in pipelines are corrosion and system disturbance due to seismic excitations [1–3] and ground movement, which arise from traffic loading, ground temperature and moisture changes, as well as adjacent excavation such as trenching or tunnelling [4–10].

Initially, experimental studies were carried out to measure the deformation of the ground and buried pipelines during the tunnelling and to provide more insight into the mechanism of soil–pipe interaction [11–14]. With the development of computer technology, a series of numerical simulations were conducted to model the experimental test and to estimate the response of a buried pipeline. The complex soil–pipeline interaction can be taken into account by numerical simulations with the complex geological and geometrical conditions and construction process in practice [15–18].

In addition to numerical simulations, analytical solutions are less time-consuming and easier for practical utilization. The interaction between the pipeline and the soil is usually analyzed by using the subgrade reaction analysis. This method assumes that the buried pipeline is an elastic beam resting on an elastic foundation model [19–22]. The beam usually uses Bernoulli–Euler beam theory in which straight lines or planes, normal to the neutral beam axis, remain straight after deformation. This theory neglects the effect of transverse shear deformations and is relevant only to slender beams. The Winkler foundation model, widely used in subgrade reaction analysis, is characterized by the

assumption that the pressure in the foundation is proportional to the deflection at the very point and is independent of pressures or deflections elsewhere. This simpler foundation model can be easily applied and gives satisfactory results in many practical situations. However, it is a rather crude approximation without considering the continuity or cohesion of the soil. Two-parameter elastic foundation models, including the Pasternak foundation model, are adopted herein to overcome this deficiency.

Meanwhile, pipelines with joints are often overlooked in related research. For the interaction analysis to be of any practical use, equal importance should be given to adequately defining the strength and deformation properties of the pipelines, their joints and the surrounding soil. Some scholars [23–28] consider the jointed pipeline as a continuous pipeline with additional local rotations at the joints. Liu et al. [29] provide a mathematical model to estimate the mechanical behaviors of the existing tunnels with bending stiffness and shearing stiffness reduction at the movement joints.

What is more, the detachment of the underlying soil potentially occurs beneath the jointed pipeline, which inevitably causes nonlinearity. Due to the unknown contact location, the detachment is highly nonlinear even in the range of small deformation and linear elastic behavior. The existing solutions to this problem are highly sophisticated mathematical analyses. Some distinct approaches may be found in the literature: direct approaches, numerical simulations and mathematical models [30–38]. To deal with the problem, a set of transcendental equations or inequalities, and an iterative technique is utilized in all approaches. The finite difference method [39–41] of the numerical approach is utilized herein, which has emerged as a powerful and effective technique to study many problems arising in beams in material mechanics.

Compared with the aforementioned research, we provide a novel mathematical model to simulate the joints on the buried pipeline. The mechanical behaviors of the buried pipeline with joints are analyzed. When calculating the buried pipeline's mechanical behaviors, the bending stiffnesses of the joint and standard pipe section are utilized separately, rather than using the equivalent bending stiffness. Additionally, the detachment potentially occurring at the bottom of the pipeline is considered. The iterative calculation is applied to discriminate whether the detachment occurs. Subgrade reaction analysis is used to obtain the numerical results by using the finite difference method. The results proposed by our method agree with the data from centrifuge tests. Parametric analyses are carried out to study the effects of the stiffness reduction factor, the coefficient of subgrade reaction, and the Pasternak shear modulus of the foundation.

2. Jointed Pipeline Subjected to Tunneling

2.1. Calculation Model of Subgrade Reaction Analysis

In the traditional methods, the pipeline is regarded as an elastic beam resting on an elastic foundation. The interaction between the soil and pipeline is taken into account by a series of independent springs. A shear layer connecting these independent springs is applied to consider the shear interaction between the springs. The tunnelling-induced ground movement adds pressure on the elastic beam. After considering the arching effect, the profile of the ground movement is described by the Gaussian distribution function.

Since most buried pipelines have joints in practice, the traditional deformation of buried jointed pipelines cannot be calculated using the beam with equivalent bending stiffness. If the joints are in the least helpful position, the mechanical behaviors of the buried pipeline will be significantly affected. Different deformation mechanisms depend on the number of joints and the relative position between the joints and the new tunnel [29]. Figure 1 shows the deformation characteristics of the jointed pipelines subjected to new tunnelling.

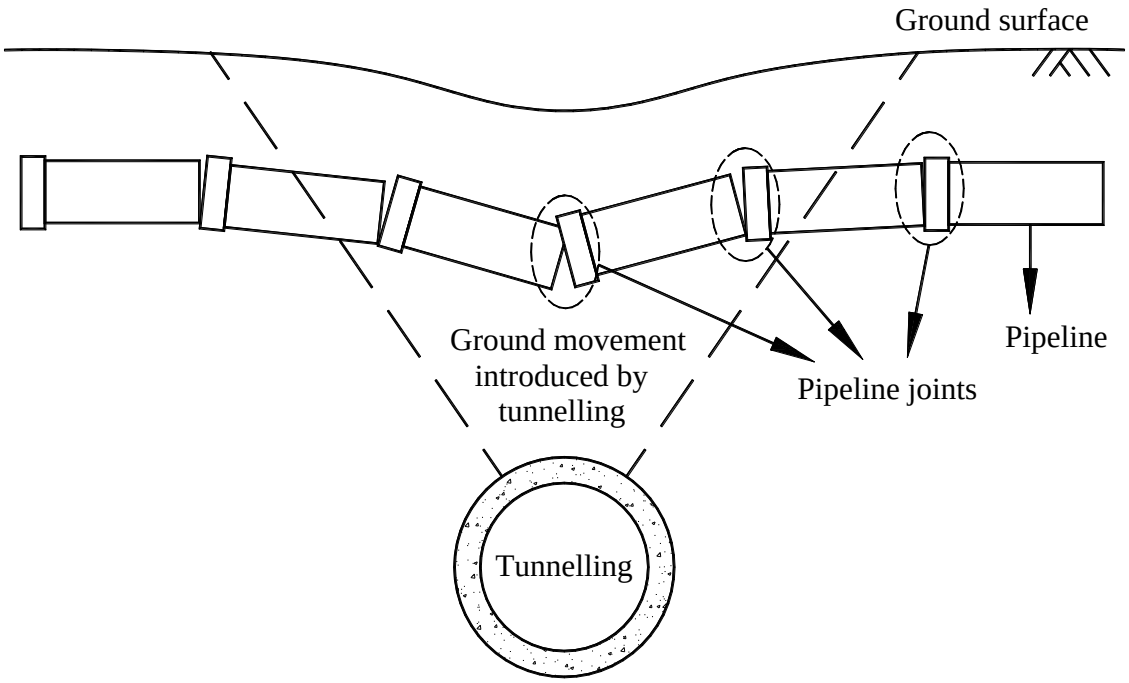

Figure 1. Typical deformation of buried jointed pipeline subjected to tunnelling-induced ground settlement while the joints are in the least helpful positions.

Figure 2 indicates the calculation model of the subgrade reaction analysis. Some assumptions required in the calculation model are detailed as follows: (1) The soil material is modeled by the Pasternak foundation model; (2) The settlement of the foundation is represented by the Gaussian function; (3) The pipe material is linearly elastic, homogeneous and isotropic; (4) The pipeline is regarded as the Bernoulli–Euler beam model because the deflections of the pipelines are small; (5) The jointed pipeline is considered as a continuous pipeline with additional moments at the joints; (6) Axial forces in the pipeline and friction on the contact surface are not taken into account; (7) Detachment is allowed between the soil and the pipeline, as shown in Figure 3. Due to the existence of the last hypothesis, both the linear and nonlinear deformation of the pipeline can be considered.

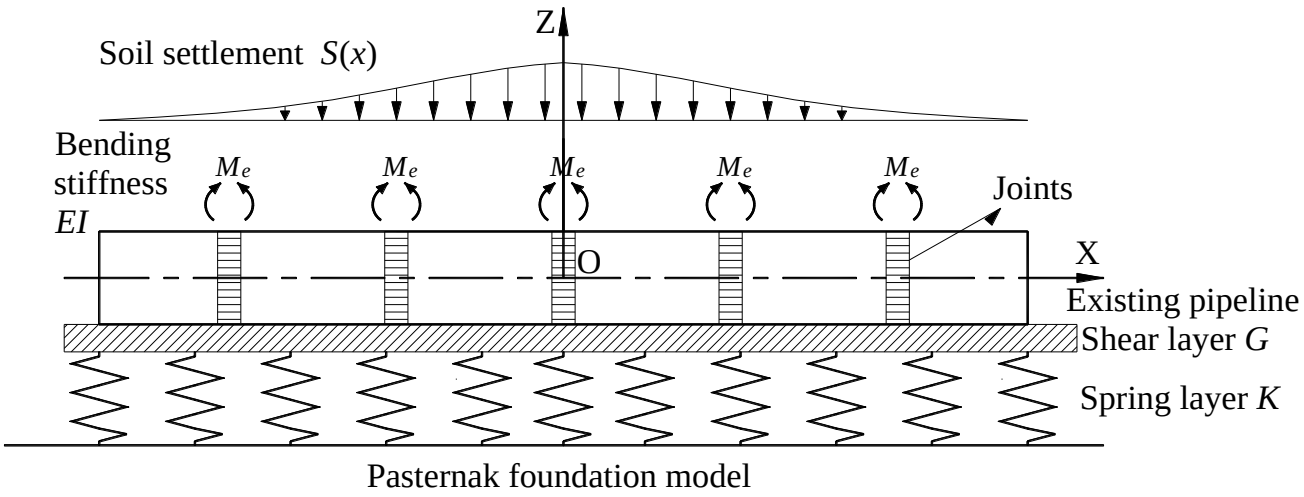

Figure 2. Calculation model of subgrade reaction analysis.

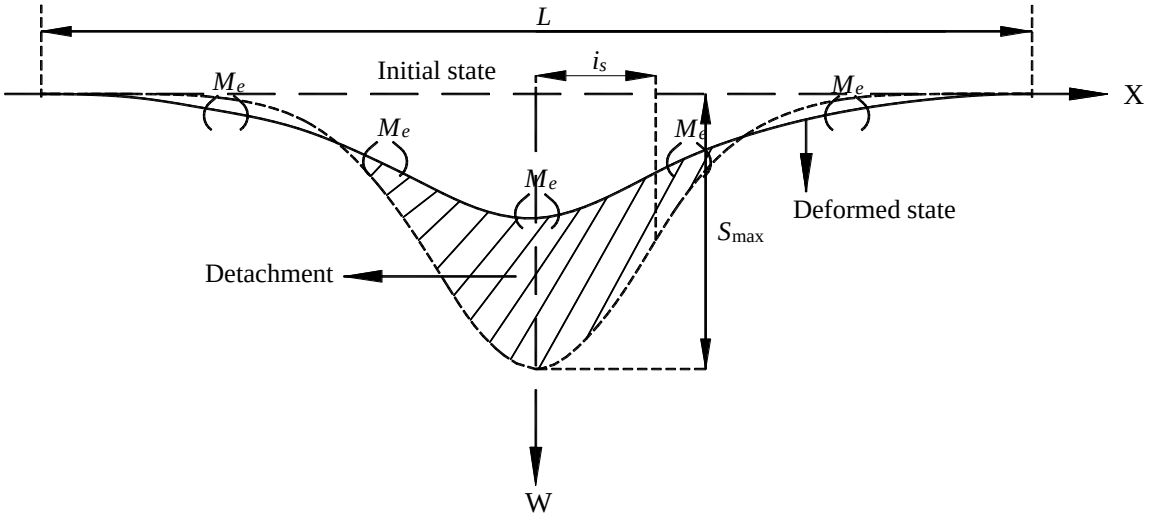

Figure 3. Detachment between underlying soil and pipeline.

The Pasternak foundation model assumes the existence of shear interactions between the spring elements. It connects the ends of the springs to a shear layer comprising incompressible vertical elements and deforms only by transverse shear, as shown in Figure 2.

The differential equation of Bernoulli–Euler beam on the Pasternak foundation is

$$EI\frac{d^4w}{dx^4} = q(x) - p(x) \tag{1}$$

where EI is the flexural rigidity of the beam; w is the deflection of the beam taking downside positive; $q(x)$ is the external load, composed of the self-weight of pipelines and covered soil and additional moment at joints; and $p(x)$ is the reaction force of the elastic foundation. To derive the constitutive relationship between the load and deflection of the foundation, the vertical equilibrium of an element in the shear layer is considered, as shown in Figure 4.

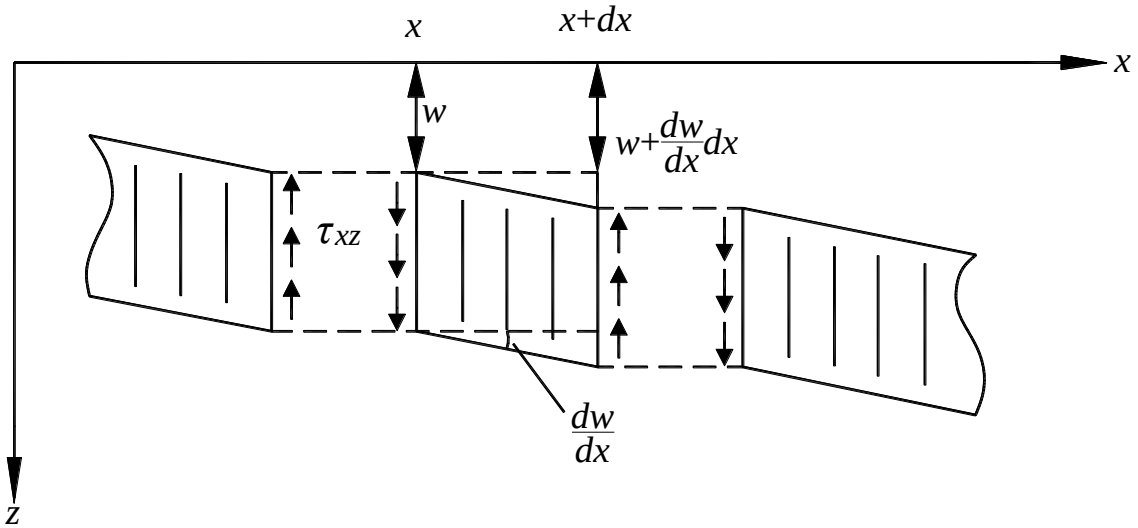

Figure 4. An element of shear layer in Pasternak foundation.

Assuming that the foundation material is homogeneous and isotropic in the $x - y$ plane, we have $G_x = G_y = G$, then

$$\tau_{xz} = G_x\gamma_{xz} = G\frac{\partial(w - S)}{\partial x} \tag{2a}$$

$$\tau_{yz} = G_y \gamma_{yz} = G\frac{\partial(w-S)}{\partial y} \tag{2b}$$

Noting that S is the tunnelling-induced ground movement described as a function of soil deflection. The deformation of the contact area is $(w - S)$. The shear forces per unit length of the shear layer are

$$N_x = \int_0^1 \tau_{xz} dz = G\frac{\partial(w-S)}{\partial x} \tag{3a}$$

$$N_y = \int_0^1 \tau_{yz} dz = G\frac{\partial(w-S)}{\partial y} \tag{3b}$$

Figure 5 shows an element in the shear layer. According to the force balance, the equilibrium equation is

$$\frac{\partial N_x}{\partial x} + \frac{\partial N_y}{\partial y} + p - q_s = 0 \tag{4}$$

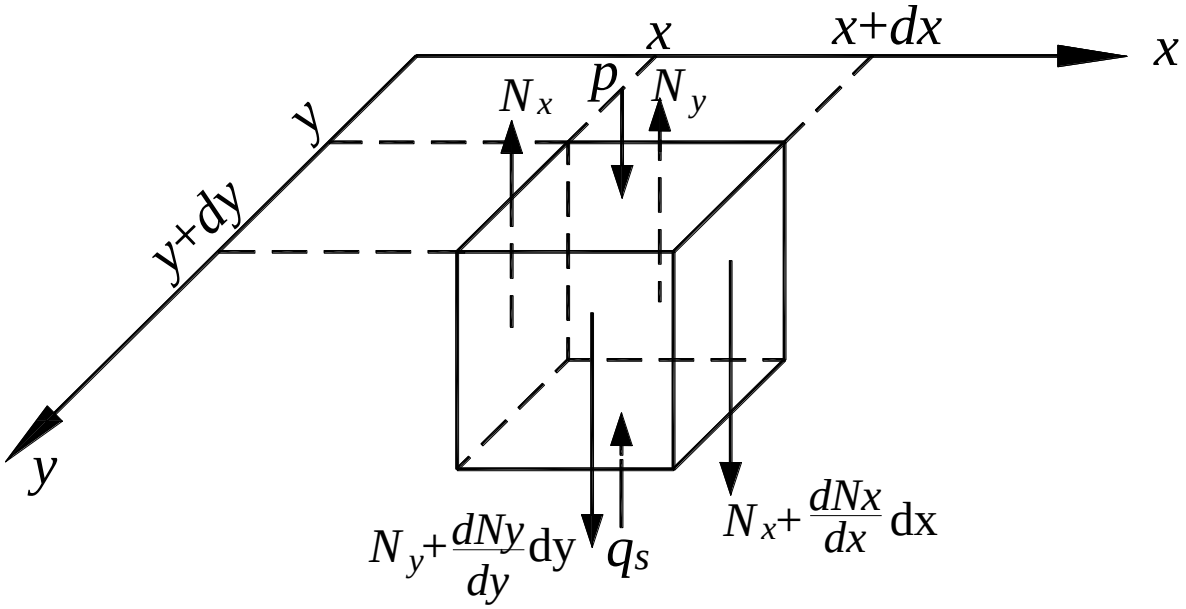

Figure 5. Vertical equilibrium of an element in the shear layer.

Substituting Equations (3a) and (3b) into Equation (4), we obtain the reaction force p with $q_s = K(w - S)$

$$p(x) = K(w-S) - G\nabla^2(w-S) \tag{5}$$

where K is the coefficient of subgrade reaction, G is the Pasternak shear modulus of the foundation and the shear modulus of the shear layer, and ∇^2 is the Laplace operator. The second term on the right-hand side of Equation (5) is the effect of the shear interactions on the vertical elements.

Substituting Equation (5) into Equation (1), the governing equation is given by

$$EI\frac{d^4w}{dx^4} + K(w-S) - G\frac{d^2(w-S)}{dx^2} = q(x) \tag{6}$$

The tunnelling-induced ground movement of the foundation can be represented mathematically by profile functions. For example, trigonometric, hyperbolic, exponential, and

Gauss error functions. The profile function used here is the most popular Perk function [42] given by Equations (7a) and (7b).

$$S(x) = S_{max} exp(-\frac{x^2}{2i_s^2}) \tag{7a}$$

$$S_{max} = \frac{V_s}{\sqrt{2\pi} i_s} \tag{7b}$$

where S_{max} is the maximum displacement, V_s is the volume of ground settlement through per unit distance of tunnel advance, i_s is the parameter defining the form and span of the settlement.

2.2. Mathematical Model of Joints and Detachment

The jointed pipeline can be considered as a continuous pipeline with additional local rotations at the joints, which can be achieved by applying additional moments at the joints as shown in Figure 2. The additional moment can be written as distributed loads with the pulse function employed

$$q_e(x) = A\delta''(x - x_j) \tag{8}$$

where $\delta(x)$ is the pulse function, as shown in Figure 6a, $\delta''(x - x_j)$ denotes second-order derivatives with respect to x, and x_j is the abscissa of the joint. $\delta''(x - x_j)$ will be simplified to δ_j'' in the following paper. The additional moment is equivalent to the limit case that three concentrated forces act around x_j while h approaches 0, as shown in Figure 6b, where

$$P_0 = (\frac{A}{8h^3}) \cdot 2h = \frac{A}{4h^2} \tag{9}$$

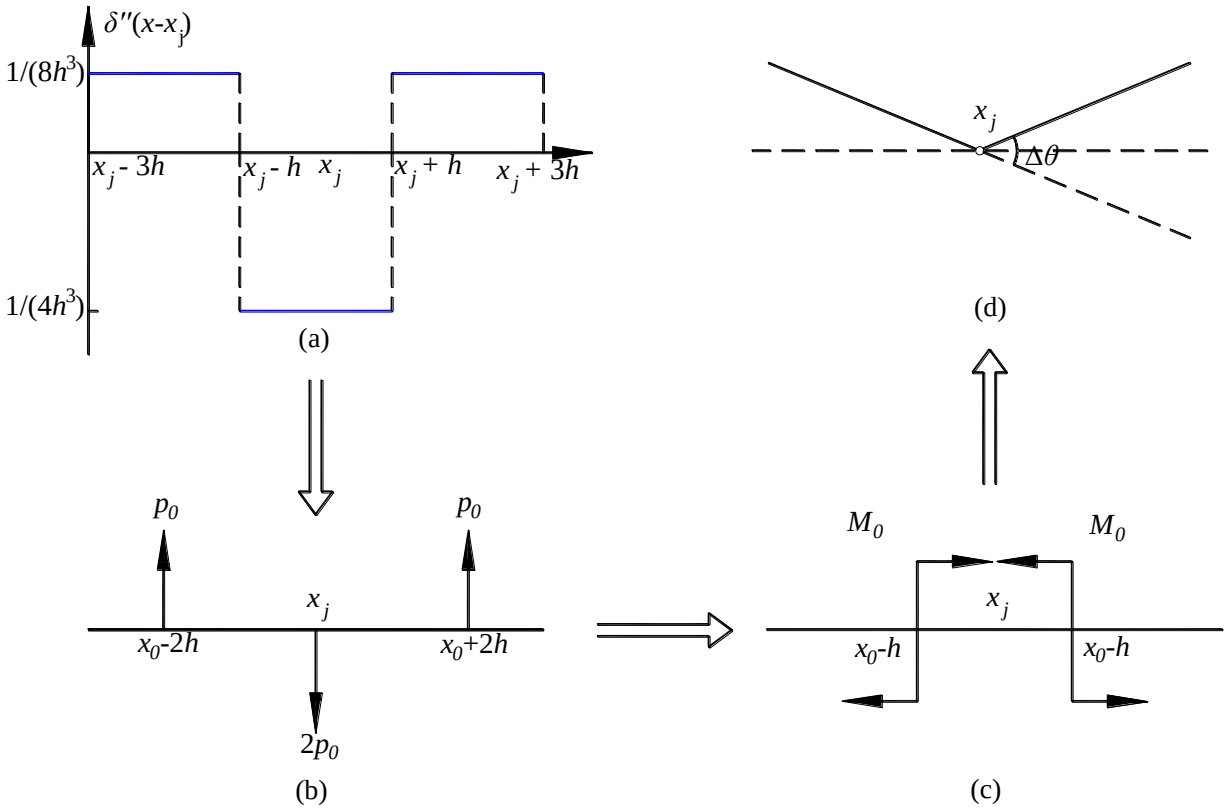

Figure 6. Additional local rotation can be realized by introducing an additional moment. (**a**) Pulse function; (**b**) Equivalent concentrated forces; (**c**) Additional moment at joints; (**d**) Related rotation at joints.

As also shown in Figure 6c, $2P_0$ is decomposed into two P_0 and combined into couples with the other P_0 on the left and right sides, where

$$M_0 = P_0 \cdot 2h = \frac{A}{2h} \tag{10}$$

The distance between the two couples is $2h$.

With additional moments applied, additional local rotations are generated while the equilibrium of the pipeline maintains unchanged. The angle of rotation is shown in Figure 6d.

$$\Delta\theta = \frac{M_e}{EI} \cdot 2h = \frac{A}{2h} \cdot \frac{2h}{EI} = \frac{A}{EI} \tag{11}$$

where M_e is the additional moment, hence

$$A = EI\Delta\theta \tag{12}$$

and

$$q_e = EI\Delta\theta\delta_j'' \tag{13}$$

while the actual rotation of the pipeline determines the additional local rotation, it can be estimated by adding a stiffness reduction factor to the continuous pipeline at each joint, and the actual moment for the jointed pipeline is

$$M(x) = EIw''(x) - M_e(x) = \begin{cases} \beta EIw''(x) & x = x_j \\ EIw''(x) & x \neq x_j \end{cases} \tag{14}$$

where β is the stiffness reduction factor. In that case,

$$M_e(x) = \begin{cases} (1-\beta)EIw''(x) & x = x_j \\ 0 & x \neq x_j \end{cases} \tag{15}$$

Taking only the self-weight of pipelines and covered soil into account, the external forces can be considered as line loads. Meanwhile, detachment, as well as additional moments, are under consideration. Equation (6) becomes

$$EI\frac{d^4w}{dx^4} + \left[k(w-S) - G\frac{d^2(w-S)}{dx^2}\right]H(x) = \gamma g + \sum_{j=1}^{N} EI\Delta\theta_j\delta_j'' \tag{16}$$

with the boundary conditions

$$\theta(0) = \theta(L) = 0, Q(0) = Q(L) = 0, S'(0) = S'(L) = 0 \tag{17}$$

where γ is the linear density, g is the gravity acceleration, and $H(x)$ is the step function defined as

$$H(x) = \begin{cases} 1 & w \geq S \\ 0 & w < S \end{cases} \tag{18}$$

2.3. Calculation Method and Procedure

The Central Difference Method (CDM) is used to obtain the numerical results. The beam and its surroundings can be divided into $n + 1$ real nodes and four fictitious nodes with step $l = L/n$, as shown in Figure 7. Central differences (CD) at the point "i" can be defined as an approximation of derivatives.

$$\frac{d^2w_i}{dx^2} = \frac{w_{i-1} - 2w_i + w_{i+1}}{l^2} \tag{19a}$$

$$\frac{d^4 w_i}{dx^4} = \frac{w_{i-2} - 4w_{i-1} + 6w_i - 4w_{i-1} + w_{i+2}}{l^4} \tag{19b}$$

$$\frac{d^2(w_i - S_i)}{dx^2} = \frac{(w_{i-1} - S_{i-1}) - 2(w_i - S_i) + (w_{i+1} - S_{i+1})}{l^2} \tag{19c}$$

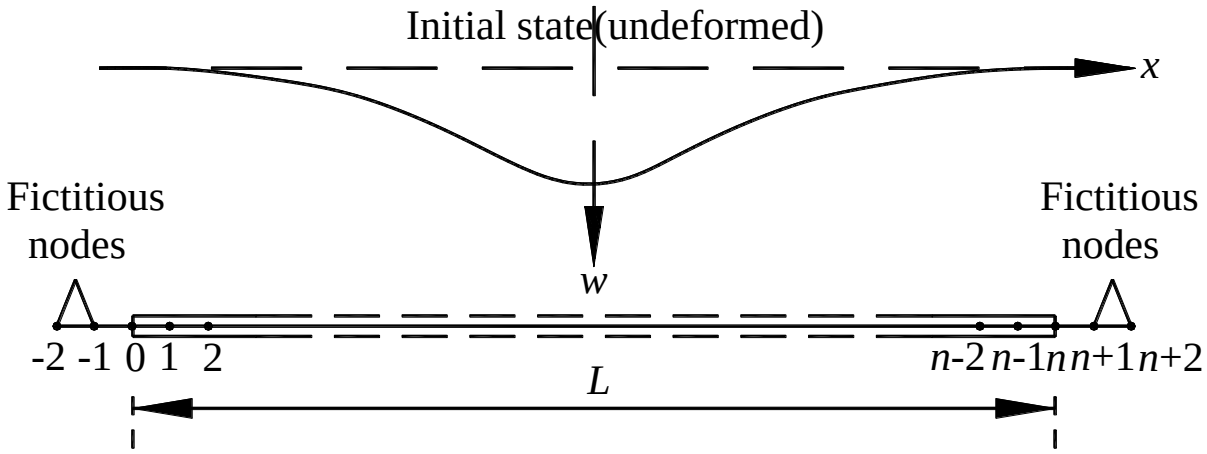

Figure 7. Divisions of the pipeline.

The additional moment at the joint is equivalent to the limit case that three concentrated forces act around the joint while h approaches0. The three concentrated forces can be applied to the joint node x_j and its adjacent nodes x_{j-1}, x_{j+1}, and $2h$ equal to l. According to Equation (11) and Equation (15), the rotation angle can be obtained by

$$M_e = \frac{EI\Delta\theta_j}{2h} = (1-\beta)EIw_j'' \tag{20}$$

$$\Delta\theta_j = (1-\beta)lw_j'' \tag{21}$$

As the number of nodes in the difference method increases, Equation (16) can be rewritten as

$$EI\frac{d^4 w}{dx^4} + \left[k(w-S) - G\frac{d^2(w-S)}{dx^2}\right]H(x) = \gamma g + (1-\beta)lEI\sum_{j=1}^{N} w_j''\delta_j'' \tag{22}$$

The three equivalence forces of the additional moment act at the joint node and its adjacent nodes. The finite difference form of Equation (22) is given by

$$\begin{cases} EI\frac{d^4 w_i}{dx^4} + \left[k(w_i - S_i) - G\frac{d^2(w_i - S_i)}{dx^2}\right]H_i = \gamma g \quad (i \neq j-1, j, j+1) \\ EI\frac{d^4 w_i}{dx^4} + \left[k(w_i - S_i) - G\frac{d^2(w_i - S_i)}{dx^2}\right]H_i = \gamma g + \frac{(1-\beta)}{l^2}lEI\sum\limits_{i=1}^{N} w_i'' \quad (i = j-1) \\ EI\frac{d^4 w_i}{dx^4} + \left[k(w_i - S_i) - G\frac{d^2(w_i - S_i)}{dx^2}\right]H_i = \gamma g - \frac{2(1-\beta)}{l^2}lEI\sum\limits_{i=1}^{N} w_i'' \quad (i = j) \\ EI\frac{d^4 w_i}{dx^4} + \left[k(w_i - S_i) - G\frac{d^2(w_i - S_i)}{dx^2}\right]H_i = \gamma g + \frac{(1-\beta)}{l^2}lEI\sum\limits_{i=1}^{N} w_i'' \quad (i = j+1) \end{cases} \tag{23}$$

Employing Equations (19a)–(19c), we have

$$\begin{gathered} EI\frac{(w_{i-2} - 4w_{i-1} + 6w_i - 4w_{i+1} + w_{i+2})}{l^4} \\ + \left[k(w_i - S_i) - G\frac{(w_{i-1} - S_{i-1}) - 2(w_i - S_i) + (w_{i+1} - S_{i+1})}{l^2}\right]H_i \\ = \gamma g \quad (i \neq j-1, j, j+1) \end{gathered} \tag{24a}$$

$$\begin{aligned} &EI\tfrac{(w_{i-2}-4w_{i-1}+6w_i-4w_{i+1}+w_{i+2})}{l^4} \\ &+\left[k(w_i-S_i)-G\tfrac{(w_{i-1}-S_{i-1})-2(w_i-S_i)+(w_{i+1}-S_{i+1})}{l^2}\right]H_i \\ &=\gamma g+\tfrac{(1-\beta)}{l^2}lEI\sum_{i=1}^{N}\tfrac{w_{i-1}-2w_i+w_{i+1}}{l^2} \quad (i=j-1) \end{aligned} \tag{24b}$$

$$\begin{aligned} &EI\tfrac{(w_{i-2}-4w_{i-1}+6w_i-4w_{i+1}+w_{i+2})}{l^4} \\ &+\left[k(w_i-S_i)-G\tfrac{(w_{i-1}-S_{i-1})-2(w_i-S_i)+(w_{i+1}-S_{i+1})}{l^2}\right]H_i \\ &=\gamma g-\tfrac{2(1-\beta)}{l^2}lEI\sum_{i=1}^{N}\tfrac{w_{i-1}-2w_i+w_{i+1}}{l^2} \quad (i=j) \end{aligned} \tag{24c}$$

$$\begin{aligned} &EI\tfrac{(w_{i-2}-4w_{i-1}+6w_i-4w_{i+1}+w_{i+2})}{l^4} \\ &+\left[k(w_i-S_i)-G\tfrac{(w_{i-1}-S_{i-1})-2(w_i-S_i)+(w_{i+1}-S_{i+1})}{l^2}\right]H_i \\ &=\gamma g+\tfrac{(1-\beta)}{l^2}lEI\sum_{i=1}^{N}\tfrac{w_{i-1}-2w_i+w_{i+1}}{l^2} \quad (i=j+1) \end{aligned} \tag{24d}$$

with boundary conditions

$$\begin{cases} \theta(0)=w'(0)=w'_0=\frac{-w_{-1}+w_1}{2l}=0 \\ \theta(L)=w'(L)=w'_n=\frac{-w_{n-1}+w_{n+1}}{2l}=0 \\ Q(0)=EIw''(0)=EIw''_0=\frac{EI(-w_{-2}+2w_{-1}-2w_1+w_2}{l^3}=0 \\ Q(L)=EIw''(L)=EIw''_n=\frac{EI(-w_{n-2}+2w_{n-1}-2w_{n+1}+w_{n+2}}{l^3}=0 \\ S'(0)=S'_0=\frac{-S_{-1}+S_1}{2l}=0 \\ S'(L)=S'_n=\frac{-S_{n-1}+S_{n+1}}{2l}=0 \end{cases} \tag{25}$$

Fictitious nodes are then eliminated

$$\begin{cases} w_{-2}=w_2 \\ w_{-1}=w_1 \\ w_{n+1}=w_{n-1} \\ w_{n+2}=w_{n-2} \\ S_{-1}=S_1 \\ S_{n+1}=S_{n-1} \end{cases} \tag{26}$$

In that case, Equations (24a)–(24d) can be simplified into matrix form:

$$[K_{EI}]\{w\}+[K_k][H]\{w\}-[K_G][H]\{w\}-[K_j]\{w\}=[F]+[K_k][H]\{S\}-[K_G][H]\{S\} \tag{27}$$

where

$$[K_{EI}]=\frac{EI}{l^4}\begin{bmatrix} 6 & -8 & 2 & & & & & 0 \\ -4 & 7 & -4 & 1 & & & & \\ & 1 & -4 & 6 & -4 & 1 & & \\ & & \ddots & \ddots & \ddots & & & \\ & & & 1 & -4 & 6 & -4 & 1 \\ & & & & 1 & -4 & 7 & 4 \\ 0 & & & & & 2 & -8 & 6 \end{bmatrix}_{(n+1)\times(n+1)} \tag{28a}$$

$$[K_k]=k\begin{bmatrix} 1 & & & & 0 \\ & 1 & & & \\ & & \ddots & & \\ & & & 1 & \\ 0 & & & & 1 \end{bmatrix}_{(n+1)\times(n+1)} \tag{28b}$$

$$[K_G] = G\begin{bmatrix} -2 & 2 & & & 0 \\ 1 & -2 & 1 & & \\ & \ddots & \ddots & \ddots & \\ & & 1 & -2 & 1 \\ 0 & & & 2 & -2 \end{bmatrix}_{(n+1)\times(n+1)} \tag{28c}$$

$$[K_j] = \frac{(1-\beta)EI}{l^4}\begin{bmatrix} 0 & & & & & & 0 \\ & 0 & & & & & \\ & & \ddots & & & & \\ & & & [C]_j & & & \\ & & & & \ddots & & \\ & & & & & 0 & \\ 0 & & & & & & 0 \end{bmatrix}_{(n+1)\times(n+1)} \tag{28d}$$

$$[C]_j = \begin{bmatrix} 1 & -2 & 1 \\ -2 & 4 & -2 \\ 1 & -2 & 1 \end{bmatrix}_{3\times 3} \tag{28e}$$

$$[F] = \gamma g l\begin{bmatrix} \frac{1}{2} & 1 & \cdots & 1 & \frac{1}{2} \end{bmatrix}_{1\times(n+1)} \tag{28f}$$

$$[H] = \begin{bmatrix} H_0 & & & & & & 0 \\ & H_1 & & & & & \\ & & \ddots & & & & \\ & & & H_i & & & \\ & & & & \ddots & & \\ & & & & & H_{n-1} & \\ 0 & & & & & & H_n \end{bmatrix}_{(n+1)\times(n+1)} \tag{28g}$$

$$H_i = \begin{cases} 1, w \geq S \\ 0, w < S \end{cases} \tag{28h}$$

$$\{w\} = [w_0 \;\; w_1 \;\; \cdots \;\; w_n]^T_{(n+1)\times 1} \tag{28i}$$

$$\{S\} = [S_0 \;\; S_1 \;\; \cdots \;\; S_n]^T_{(n+1)\times 1} \tag{28j}$$

We have

$$\left([K_{EI}] + [K_k][H] - [K_G][H] - [K_j]\right)\{w\} = [F] + ([K_k][H] - [K_G][H])\{S\} \tag{29}$$

Hence

$$\{w\} = \left([K_{EI}] + [K_k][H] - [K_G][H] - [K_j]\right)^{-1}([F] + ([K_k][H] - [K_G][H])\{S\}) \tag{30}$$

Since this paper does not involve large deformations and nonlinear constitutive relationships, the usual iteration strategies, such as the Newton–Raphson method, could be applied to address the simple contact problem. In order to reach the initial solution, we need to initialize the problem first, and reduce the unilateral contact case to a bilateral contact one. An iterative process is repeated until a convergence criterion is achieved. The calculation procedure described previously is summarized in Figure 8.

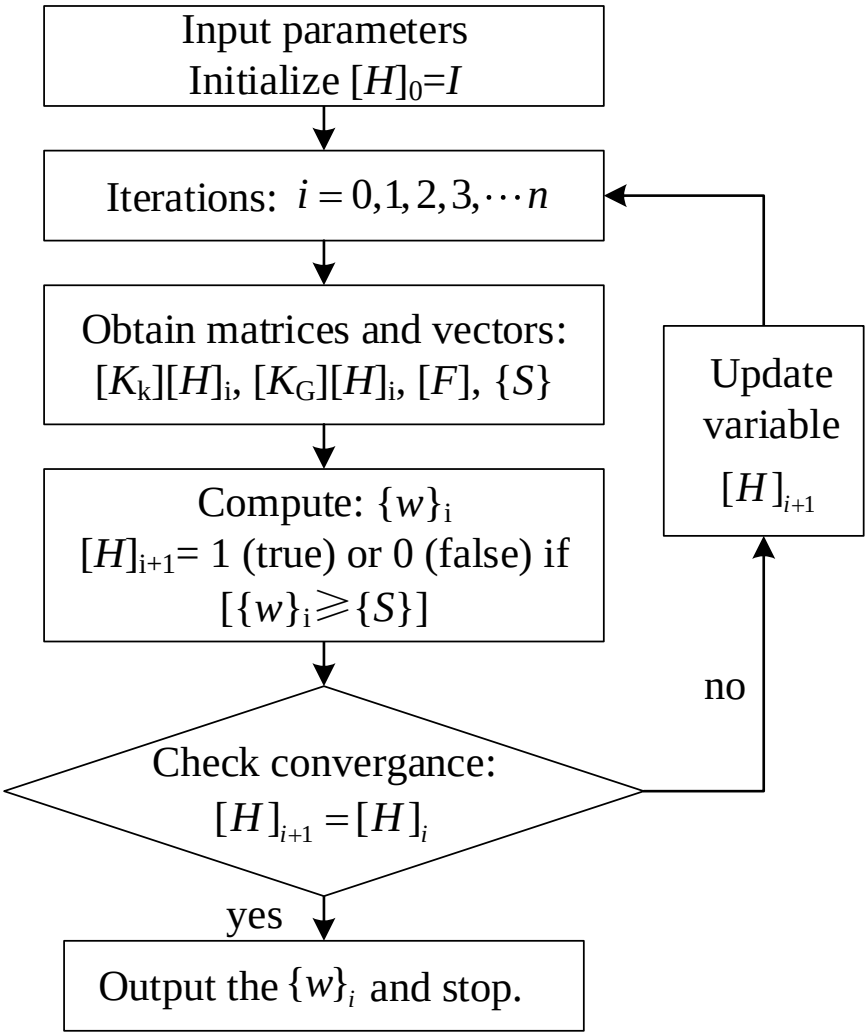

Figure 8. Nonlinear solution procedure based on Newton–Raphson method.

First, input the calculation parameters and initialize the matrix [*H*] as the identity matrix. Second, obtain the matrices and vectors in Equation (30). Third, compute the displacement vector {*w*} and compare the vector {*w*} with the vector {*S*} to obtain [*H*] as in Equation (28h). Fourth, update [*H*] and recalculate {*w*} until the convergence criterion is achieved.

3. Verification from Centrifuge Tests

In this section, two centrifuge tests conducted by Vorster et al. [43] are used to verify our proposed method. A pipeline modeled in the centrifuge tests had nine joints, and the middle joint was located directly above a new tunnel. The jointed pipeline was made of aluminum alloy with 1.22 mm thickness and 15.85 mm outer diameter, and was subjected to tunnelling-induced ground movement. The model tunnel, with 60 mm diameter, was modeled and filled with water to induce a given volume loss by extracting water. The volume loss ratio was set at 0.3% and 2.0% in Test 1 and Test 2, respectively, performed under 75 *g* acceleration. Table 1 shows the calculation parameters of the prototype scenario. The stiffness reduction factor is considered to be zero. Figures 9 and 10 show the experimental data of centrifuge tests, the calculated deflections, and the comparison with the analytical results calculated by other methods.

Table 1. Geometrical and physical parameters of centrifuge tests and analytical methods (Vorster, [43]; Liu et al. [29]).

Pipeline	D (m)	L (m)	E (GPa)	I (m^4)	EI (10^9 $Nm^{2.3}$)	z_p (m)	V_l (%)	
							Test 1	Test 2
	1.19	48.06	70	0.0474	3.3149	4.165	0.3	2
Tunnel	R_0 (m)	Z_0 (m)		**Soil**	E_s (MPa)	μ	K	G_c
	2.25	11.25			10	0.3	0.7	10D

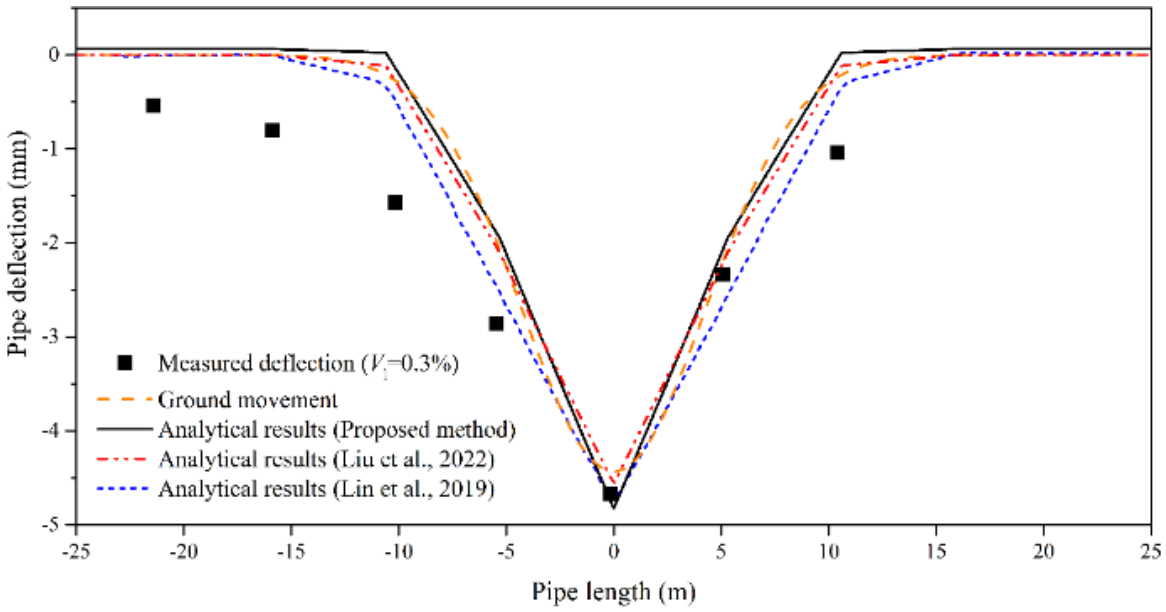

Figure 9. Verification and comparison for Test 1.

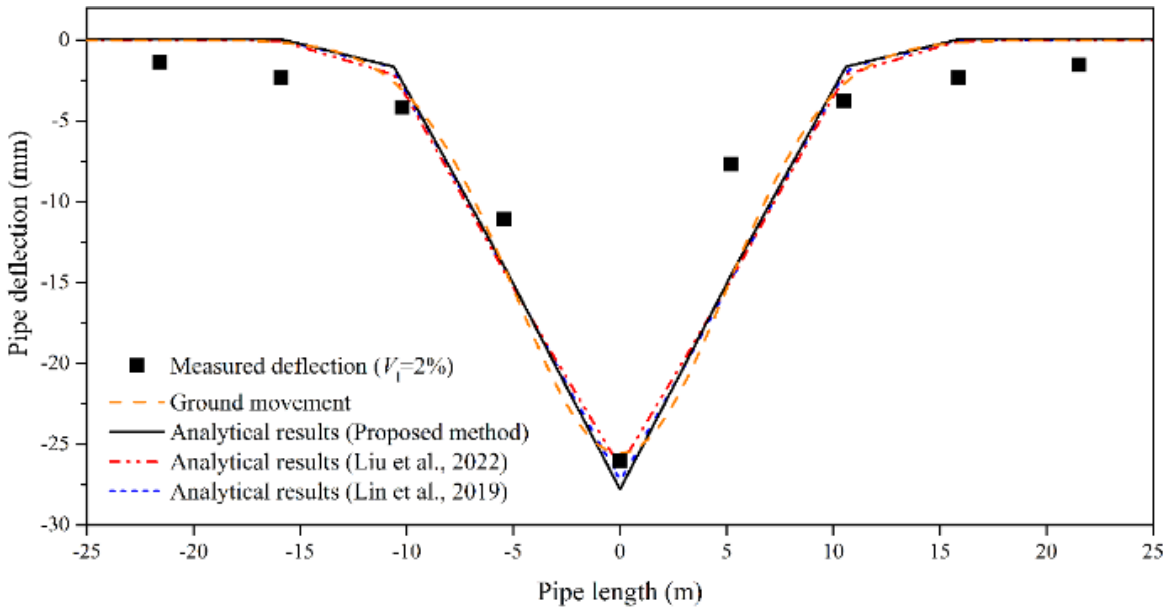

Figure 10. Verification and comparison for Test 2.

Figures 9 and 10 indicate that the calculated results proposed by our method agree with the experimental data. The profiles of pipeline deflection obtained by Liu et al. [29], Lin et al. [28], and our proposed method are similar. Lin et al. [28] provided an analytical

method without considering the variable stiffness reduction in the joints. In contrast, Liu et al. [29] consider both the rotation (bending moment) and dislocation (shearing force) with variable stiffness reduction factors, but without considering the separation between the existing tunnels and underlying soil. For Test 1, the curve's width by Lin et al. [28] is slightly wider than those of the others. For Test 2, the curve's width results are close in all three methods. The maximum deflections by our method are slightly larger than those of the others for Test 1 and Test 2.

The proposed method can calculate the deflection of the existing pipelines with joints and predict the potential detachment of the buried pipeline. As shown in Figures 9 and 10, our method is applicable for estimating the deflection of the existing pipelines with joints. Thus, our proposed method can be used to study the effects of tunnelling-induced ground movement on pipelines with joints and detachment.

4. Parametric Analyses

A calculation example is used to study the effects of the stiffness reduction factor, the coefficient of subgrade reaction, and the Pasternak shear modulus of the foundation on the deflection and bending moment of the buried pipeline.

Figure 11 shows a pipeline of length L = 30 m with joints at x = −10 m, −5 m, 0 m, 5 m, and 10 m, $E = 2 \times 10^{11}$ Pa. The inner diameter of the pipe is 0.43 m, and the outer diameter of the pipe is 0.46 m, γ = 90 Kg/m, g = 9.8 m/s^2, i_s = 3 m, S_{max} = 3 mm. The results were analyzed by the MATLAB program.

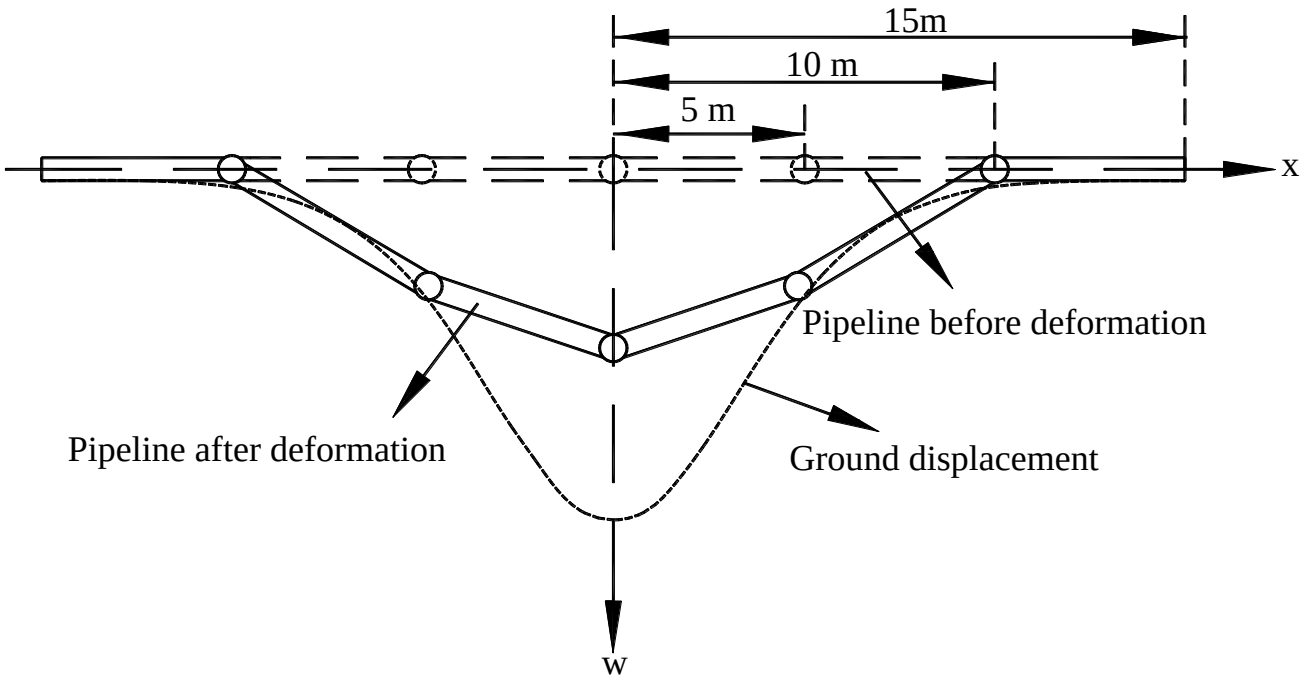

Figure 11. Example of buried jointed unilateral pipeline.

4.1. Stiffness Reduction Factor

To obtain the results by our proposed method, different stiffness reduction factors β of 0.05, 0.1, 0.5, and 1 were used., The coefficient of subgrade reaction K is 50 MPa, and the Pasternak shear modulus is 10 MPa. The pipeline is completely continuous, and the joints have no effect on it when β = 1. Figure 12 shows the deflection and bending moment of the jointed pipeline.

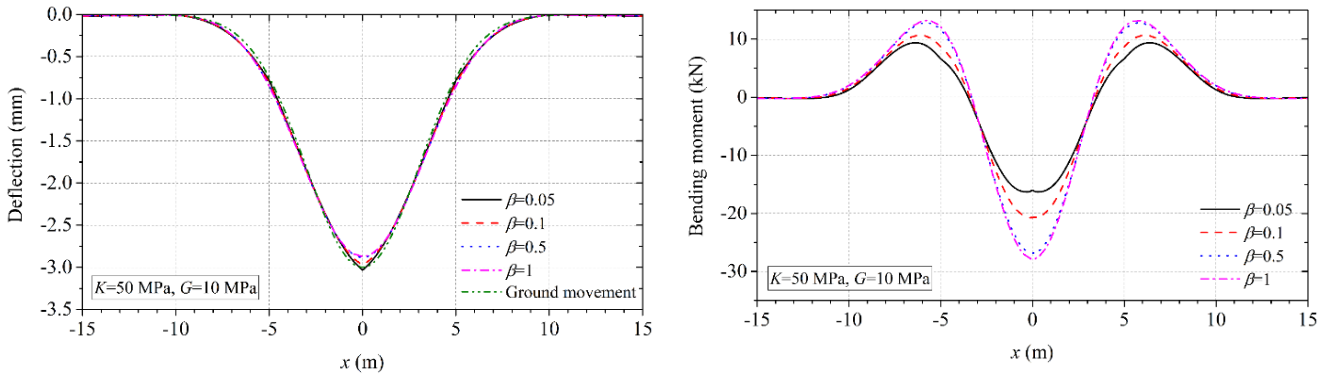

(**a**) (**b**)

Figure 12. Deflection and bending moment of buried pipeline with different stiffness reduction factors: (**a**) deflection; (**b**) bending moment.

As shown in Figure 12, the deflection decreases with the increased β. The discontinuous behavior at the joints, e.g., the middle joint, is more obvious with the decreased β. The minimum deflection at the middle joint is 2.87 mm, less than S_{max} = 3 mm. The detachment beneath the middle joint occurs, whereas it does not occur when β is less than 0.05. The bending moment increases with the increase in β. The profiles of the bending moment are similar. In contrast, the curve at the joints (x = −5 m, 0 m, 5 m) is remarkably discontinuous when β is 0.05. So, the stiffness reduction factor β is of great significance to represent the discontinuous behavior of the pipeline.

4.2. Coefficient of Subgrade Reaction

Figure 13 shows the deflection and bending moment of the buried pipeline with different coefficients of subgrade reaction. The value of K was set as 10 MPa, 30 MPa, and 50 MPa, respectively. Note that the Pasternak shear modulus of foundation is 10 MPa, and β is considered as zero to make the results remarkable.

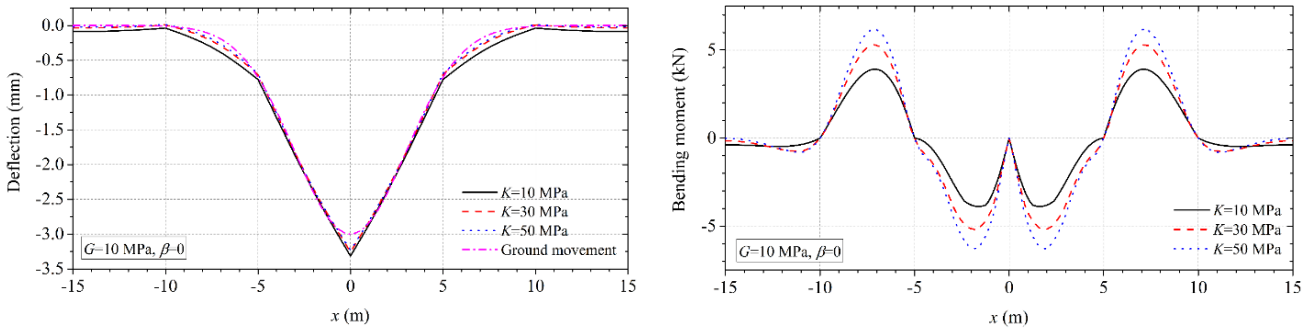

(**a**) (**b**)

Figure 13. Deflection and bending moment of buried pipeline with different coefficients of subgrade reaction: (**a**) deflection; (**b**) bending moment.

As shown in Figure 13, the deflection increases slightly with the decrease in the coefficient of subgrade reaction. The maximum deflection is 3.23 mm, larger than S_{max} = 3 mm. The buried pipeline maintains contact with the underlying soil. The discontinuous behavior of the jointed pipeline is remarkable with the decreased K. The bending moment increases with the increased coefficient of subgrade reaction. The middle sections of the pipeline, from −10 m to 10 m, generate large bending moments. By contrast, the bending moment of the joints at x = −10 m, −5 m, 0 m, 5 m, and 10 m are all zero because the bending stiffness of the joints is zero due to Equation (14). The results indicate apparent discontinuous changes at the joints.

4.3. Pasternak Shear Modulus of Foundation

To study the effects of the Pasternak shear modulus of foundation, we set G to be 10 MPa, 30 MPa, and 50 MPa, respectively. The coefficient of subgrade reaction and the stiffness reduction factor are 50 MPa and 0, respectively. The deflection and bending moment of the buried pipeline are shown in Figure 14.

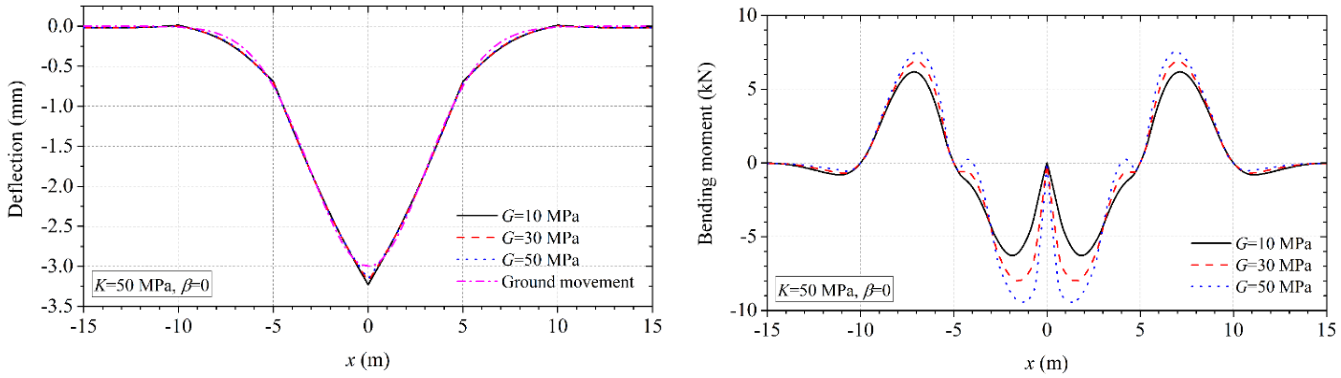

(**a**) (**b**)

Figure 14. Deflection and bending moment of buried pipeline with different Pasternak shear moduli of foundation: (**a**) deflection; (**b**) bending moment.

The deflection increases slightly with the decrease in the Pasternak shear modulus of foundation. The maximum deflection is 3.32 mm and occurs at the middle joint. The effect of the Pasternak shear modulus of foundation G on the discontinuous deflection of the pipeline is not significant except for the middle joint. The zero stiffness reduction factor results in larger deflections than the ground movements, so the buried pipeline maintains contact with the underlying soil. The bending moment increases with the increased Pasternak shear modulus of foundation. The characteristics of the results are consistent with those of the coefficient of subgrade reaction.

5. Conclusions

We propose an analytical method to estimate the deflection and bending moment of the jointed pipeline and its detachment. The pipeline is regarded as an elastic beam resting on a Pasternak foundation model. Our proposed method is verified by the centrifuge tests when compared with other methods. Parametric analyses about the main influencing factors are carried out and the findings are as follows:

- We provide a mathematical model which uses the pulse function to model the joints and uses the iteration method to determine the detachment. The deflections of the jointed pipeline calculated by our method agree with the experimental data which indicates our proposed method's reasonability.
- The maximum value and profile of the pipeline's deflection obtained by our method are close to those calculated by the other methods. Our method can not only predict the deflections of the jointed pipeline, but also determine whether the detachment occurs.
- The deflections of the jointed pipeline increase with the decrease in the stiffness reduction factor β, the coefficient of subgrade reaction K, and the Pasternak shear modulus of foundation G, whereas the bending moments decrease. The stiffness reduction factor is of great significance to the discontinuous behavior of the jointed pipeline.
- Detachment beneath the jointed pipeline sometimes happens and sometimes does not, depending on our proposed method's iteration. Thus, more attention should be paid to the detachment between the pipeline and underlying soil.

Author Contributions: Conceptualization, X.L. and Y.D.; methodology, Y.D. and X.L.; software, X.L.; validation, X.L. and R.Z.; formal analysis, Y.D.; investigation, Y.D.; resources, C.Y.; data curation, R.Z.; writing—original draft preparation, Y.D.; writing—review and editing, X.L.; supervision, X.L.; project administration, C.Y.; funding acquisition, X.L. All authors have read and agreed to the published version of the manuscript.

Funding: The authors gratefully acknowledge the financial support by the National Natural Science Foundation of China under Grant 52108363 and the China Postdoctoral Science Foundation under grant number 2021M700654.

Institutional Review Board Statement: Not applicable.

Informed Consent Statement: Informed consent was obtained from all subjects involved in the study.

Conflicts of Interest: The authors declare no conflict of interest.

References

1. Maleska, T.; Nowacka, J.; Beben, D. Application of EPS geofoam to a soil-steel bridge to reduce seismic excitations. *Geosciences* **2019**, *9*, 448. [CrossRef]
2. Mahgoub, A.; Naggar, H.E.I. Seismic design of metal arch culverts: Design codes vs. full dynamic analysis. *J. Earthq. Eng.* **2019**, *25*, 2231–2268. [CrossRef]
3. Liu, X.; Jiang, A.N.; Guo, X.; Hai, L. Effect of excavation blasting in the arch cover method on adjacent existing pipelines in a subway station. *Appl. Sci.* **2022**, *12*, 1529. [CrossRef]
4. O'Rourke, T.D.; Trautmann, C.H. Buried pipeline response to tunneling ground movements. *Europipe* **1982**, *82*, 9–15.
5. Carder, D.R.; Taylor, M.E. *Response of a Pipeline to Nearby Deep Trenching in Boulder Clay*; Trrl Laboratory Report; Transport and Road Research Laboratory (TRRL): Wokingham, UK, 1983.
6. Takagi, N.; Shimamura, K.; Nishio, N. Buried Pipe Responses to Adjacent Ground Movements Associated with Tunneling and Excavations. Ground Movements and Structures. In Proceedings of the 3rd International Conference, Cardiff, Wales, 1–3 April 1985.
7. Attewell, P.B.; Yeates, J.; Selby, A.R. Soil movements induced by tunneling and their effects on pipelines and structures. *Tunn. Undergr. Space Technol.* **1987**, *2*, 102.
8. Vorster, T.E.; Klar, A.; Soga, K.; Mair, R.J. Estimating the Effects of Tunneling on Existing Pipelines. *J. Geotech. Geoenvironmental Eng.* **2005**, *131*, 1399–1400. [CrossRef]
9. Klar, A.; Vorster, T.E.; Soga, K.; Mair, R.J. Soil—Pipe interaction due to tunneling: Comparison between Winkler and elastic continuum solutions. *Géotechnique* **2005**, *55*, 461–466. [CrossRef]
10. Yoo, C.S.; Choi, B.S.; Jung, H.Y. Excavation-Induced Buried Pipeline Failure—A Case Study. *Solid State Phenom.* **2006**, *110*, 23–30. [CrossRef]
11. Abuhjar, O.; Naggar, H.E.I.; Newson, T. Numerical modeling of soil and surface foundation pressure effects on buried box culvert behavior. *J. Geotech. Environ. Eng.* **2016**, *142*, 04016072. [CrossRef]
12. Yan, K.; Zhang, J.; Wang, Z.; Liao, W.; Wu, Z. Seismic responses of deep buried pipeline under non-uniform excitations from large scale shaking table test. *Soil Dyn. Earthq. Eng.* **2018**, *113*, 180–192. [CrossRef]
13. Shi, J.W.; Wang, Y.; Ng, C.W. Three-dimensional centrifuge modeling of ground and pipeline response to tunnel excavation. *J. Geotech. Environ. Eng.* **2016**, *142*, 04016045. [CrossRef]
14. Zhu, Y.T.; Zhang, H.; Zhang, Z.X.; Huang, X.; Liu, K. Physical model test study of influence of advance of shield tunnel on adjacent underground pipelines. *Rock Soil Mech.* **2016**, *37* (Suppl. S2), 151–160. (In Chinese)
15. Maleska, T.; Beben, D.; Nowacka, J. Seismic vulnerability of a soil-steel composite tunnel-Norway Tolpinrud Railway Tunnel case study. *Tunn. Undergr. Space Technol.* **2021**, *110*, 103808. [CrossRef]
16. Wang, Y.; Shi, J.; NgCharles, W.W. Numerical modeling of tunneling effect on buried pipelines. *Can. Geotech. J.* **2011**, *48*, 1125–1137. [CrossRef]
17. Wang, Z.X.; Miu, L.C.; Wang, R.R.; Pan, H. Model test study of vertical buried continuous pipelines displacements affected by tunnelling in sand. *Rock Soil Mech.* **2013**, *34* (Suppl. S2), 143–149. (In Chinese)
18. Wham, B.P.; Argyrou, C.; O'Rourke, T.D. Jointed pipeline response to tunneling induced ground deformation. *Can. Geotech. J.* **2016**, *53*, 1794–1806. [CrossRef]
19. Hetenyi, M. *Beams on Elastic Foundations*; University of Michigan Press: Ann Arbor, MI, USA, 1946.
20. Timoshenko, S.P.; Woinowsky-Krieger, S. *Theory of Plates and Shells*, 2nd ed.; McGraw-Hill: New York, NY, USA, 1959; pp. 259–281.
21. Kerr, A.D. Elastic and viscoelastic foundation models. *J. Appl. Mech.* **1964**, *33*, 491–498. [CrossRef]
22. Selvadurai, A.P.S. Elastic Analysis of Soil-Foundation Interaction. *Dev. Geotech. Eng.* **1979**, *16*, 38. [CrossRef]
23. Singhai, A.C. Behavior of Jointed Ductile Iron Pipelines. *J. Transp. Eng.* **1984**, *110*, 235–250. [CrossRef]
24. Becerril, García, D.; Moore, I.D. Behaviour of bell and spigot joints in buried reinforced concrete pipelines. *Can. Geotech. J.* **2015**, *52*, 609–625. [CrossRef]

25. Marshall, A.M.; Klar, A.; Mair, R.J. Tunneling beneath buried pipes: View of soil strain and its effect on pipeline behavior. *J. Geotech. Geoenviron. Eng.* **2010**, *136*, 1664–1672. [CrossRef]
26. Huang, M.S.; Zhou, X.C.; Yu, J.; Leung, C.F.; Tan, J.Q.W. Estimating the effects of tunnelling on existing jointed pipelines based on Winkler model. *Tunn. Undergr. Space Technol.* **2019**, *86*, 89–99. [CrossRef]
27. Shen, S.L.; Wu, H.N.; Cui, Y.J.; Yin, Z.Y. Long-term settlement behaviour of metro tunnels in the soft deposits of Shanghai. *Tunn. Undergr. Space Technol.* **2014**, *40*, 309–323. [CrossRef]
28. Lin, C.G.; Huang, M.S. Tunnelling-induced response of a jointed pipeline and its equivalence to a continuous structure. *Soils Found* **2019**, *59*, 828–839. [CrossRef]
29. Liu, X.; Fang, Q.; Jiang, A.; Li, J. Deformation analysis of existing tunnels with shearing and bending stiffness reduction at movement joints. *Tunn. Undergr. Space Technol.* **2022**, *123*, 104408. [CrossRef]
30. Zhang, Y.; Murphy, K.D. Response of a finite beam in contact with a tensionless foundation under symmetric and asymmetric loading. *Int. J. Solids Struct.* **2004**, *41*, 6745–6758. [CrossRef]
31. Silveira, R.A.M.; Pereira, W.L.A.; Gonçalves, P.B. Constrained and unconstrained optimization formulations for structural elements in unilateral contact with an elastic foundation. *Math. Prob. Eng.* **2008**, *2008*, 2684–2693. [CrossRef]
32. Zhang, Y. Tensionless contact of a finite beam resting on Reissner foundation. *Int. J. Mech. Sci.* **2008**, *50*, 1035–1041. [CrossRef]
33. Zhang, Y.; Murphy, K.D. Tensionless contact of a finite beam: Concentrated load inside and outside the contact zone. *Acta Mech. Sin.* **2013**, *29*, 836–839. [CrossRef]
34. Ioakimidis, N.I. Derivation of feasibility conditions in engineering problems under parametric inequality constraints with classical Fourier elimination. *Int. J. Numer. Meth. Eng.* **2015**, *48*, 1583–1599. [CrossRef]
35. Deck, O.; Singh, A. Analytical model for the prediction of building deflections induced by ground movements. *Int. J. Numer. Anal. Mech. Geomech.* **2012**, *36*, 62–84. [CrossRef]
36. Franza, A.; Deck, O.; DeJong, M.J. Charts for the mining-induced deflection of buildings. *Can. Geotech. J.* **2020**, *57*, 2020–2026. [CrossRef]
37. Franza, A.; DeJong, M.J. Elasoplastic solutions to predict tunneling-induced load redistribution and deformation of surface structures. *J. Geotech. Geoenviron. Eng.* **2009**, *145*, 04019007. [CrossRef]
38. Liu, X.; Jiang, A.N.; Hai, L.; Li, J. Study on soil gap formation beneath existing underground structures due to new excavation below. *Comput. Geotech.* **2021**, *139*, 104379. [CrossRef]
39. Frydrýšek, K.; Michenková, Š.; Nikodým, M. Straight Beams Rested on Nonlinear Elastic Foundations—Part 1 (Theory, Experiments, Numerical Approach). *Appl. Mech. Mater.* **2014**, *684*, 11–20. [CrossRef]
40. Michenková, Š.; Frydrýšek, K.; Nikodým, M. Straight Beams Rested on Nonlinear Elastic Foundations—Part 2 (Numerical Solutions, Results and Evaluation). *Appl. Mech. Mater.* **2014**, *684*, 21–29. [CrossRef]
41. Chen, X.L.; Yang, Q.H.; Ding, J.P. Mechanical Characterization of Beams on Tensionless Foundation Materials. *Mater. Sci. Forum* **2016**, *867*, 152–156. [CrossRef]
42. Peck, R. Deep Excavations and Tunneling in Soft Ground. In Proceedings of the 7th International Conference on Soil Mechanics and Foundation Engineering, Mexico City, Mexico, 25–29 August 1969; pp. 311–375.
43. Vorster, T.E.B. Effects of Tunnelling on Buried Pipes. Ph.D Thesis, University of Cambridge, Cambridge, UK, 2006.